Annals of Nuclear Medicine Vol. 11, No. 3, 233–241, 1997

Noninvasive identification of left ventricular involvements in arrhythmogenic right ventricular dysplasia: Comparison of ^{123}I-MIBG, ^{201}TlCl, magnetic resonance imaging and ultrafast computed tomography

Nobukazu TAKAHASHI,* Yoshio ISHIDA,* Masakazu MAENO,* Yoshiaki HIROSE,* Shigeo KAWANO,* Shyuji FUKUOKA,* Kohei HAYASHIDA,* Sachio KURIBAYASHI,* Seiki HAMADA,* Naoaki YAMADA,* Makoto TAKAMIYA,* Katuro SHIMOMURA** and Tohru OHE***

*Departments of Radiology and **Cardiology, National Cardiovascular Center
***Department of Cardiovascular Medicine,
Okayama University Medical School

We examined the feasibility of myocardial ^{123}I-MIBG, ^{201}TlCl, magnetic resonance imaging (MRI) and ultrafast computed tomography (UFCT) for the early detection of left ventricular involvements in 15 patients with arrhythmogenic right ventricular dysplasia (ARVD). Radionuclide ventriculography (RNV) and myocardial imaging with ^{123}I-MIBG, ^{201}TlCl, MRI and UFCT were performed in all 15 patients and in 10 normal subjects.

The patients' scans were visually interpreted by two nuclear medicine physicians taking into consideration the extent score (ES) and severity score (SS) calculated by using the bull's-eye view in relation to normal data derived from the normal subjects. The left ventricular ejection fraction (LVEF) was measured by RNV. Fourteen (93%) patients showed regional ^{123}I-MIBG defects, while 12 (80%) patients showed regional ^{201}TlCl defects. The ES and SS were higher in ^{123}I-MIBG than ^{201}TlCl (ES: 31.5 ± 18.5 vs. 17.5 ± 18.2, $p<0.01$, SS: 34.8 ± 42.2 vs. 16.9 ± 37.5, $p<0.01$). Abnormal UFCT and MRI findings suggesting fatty involvements of the LV myocardium were demonstrated in 7 patients (Group B), while 7 patients showed regional ^{123}I-MIBG defects without abnormal UFCT and MRI findings (Group A). ^{123}I-MIBG was significantly more sensitive than UFCT and MRI ($p<0.05$), although one patient, an exception, showed abnormal UFCT findings for the apex of the LV myocardium without abnormal ^{123}I-MIBG and MRI findings. The LVEF, as a measure of LV systolic function, was better preserved in Group A than in Group B (59.3 ± 3.6 vs. 45.8 ± 5.8, $p<0.01$).

The present findings indicated that myocardial imaging with ^{123}I-MIBG sensitively detects myocardial damage in patients with ARVD in the early stage when cardiac systolic function is still preserved.

Key words: arrhythmogenic right ventricular dysplasia, ^{123}I-MIBG, ^{201}TlCl, magnetic resonance imaging, ultrafast computed tomography imaging

INTRODUCTION

ARRHYTHMOGENIC RIGHT VENTRICULAR DYSPLASIA (ARVD) has been characterized as an underlying structural fibrolipomatous infiltration abnormality with degeneration of the right ventricular (RV) myocardium.[1,2]

In patients with ARVD, the frequent provocation of arrhythmias during exercise and the catecholamine sensitivity of ventricular tachycardia (VT), suggest the involvement of the autonomic nervous system in the arrhythmogenesis in this dysplasia.[3,4] I-123 metaiodobenzyl-guanidine (^{123}I-MIBG) can be used to measure postganglionic presynaptic noradrenaline uptake and is a useful method for the noninvasive *in vivo* investigation of sympathetic activity in humans.[5–11]

ARVD is considered to be a disease that primarily affects the right ventricle, but in ARVD, abnormal ^{123}I-

Received March 10, 1997, revision accepted June 25, 1997.
For reprint contact: Nobukazu Takahashi, M.D., Department of Radiology, National Cardiovascular Center, 5–7–1 Fujishirodai, Suita, Osaka 565, JAPAN.

Table 1 Clinical profiles of 15 ARVD patients

Pt. No.	Age (yr)/Sex	Chief complaint	ECG	Clinical VT	VT focus	RV biopsy
			Inverted T			
1	25/F	Syncope	V_1	NSVT	RVOT	fibrosis
2	47/M	Syncope	V_1, V_2	SVT	RVOT	fat, fibrosis
3	38/F	Syncope	—	NSVT	RVOT	fibrosis
4	65/M	Syncope	V_1	SVT	RVOT	fat, fibrosis
5	41 /M	Syncope	V_1–V_4	SVT	RVOT	fat, fibrosis
6	66/F	Syncope	V_1–V_3	SVT	RVOT	fat, fibrosis
7	39/M	Palpitation	—	NSVT	RVOT	fibrosis
8	24/F	Syncope	—	NSVT	RVOT	fat, fibrosis
9	18/M	Palpitation	V_1–V_5	SVT	undefined	fibrosis
10	33/M	Syncope	V_1, V_2	SVT	undefined	fat, fibrosis
11	40/M	Palpitation	V_1–V_4	SVT	RVIF	fat, fibrosis
12	52/M	Syncope	V_1–V_4	SVT	RVOT	fat, fibrosis
13	53/F	Syncope	V_1–V_3	SVT	undefined	not done
14	50/M	Syncope	V_1–V_4	SVT	RVIF	fat, fibrosis
15	44/M	Syncope	V_5, V_6	SVT	undefined	fat, fibrosis

M = male; F = female; ECG = electrocardiography; VT = ventricular tachycardia; NSVT = nonsustained VT; SVT = sustained VT; RV = right ventricle; RVOT = right ventricular outflow tract; RVIF right ventricular inflow tract

MIBG uptake is frequently noted in the septal left ventricle,[12,13] and functional abnormalities of the left ventricular (LV) myocardium indicating LV involvements have been observed in the more advanced stages of the disease.[14] Histologically, a pattern of widespread massive fatty infiltration and fibrosis with very few myocardial cells has been detected in the LV myocardium.[1,15] Recently, Lerch and Wichter reported that ^{123}I-MIBG imaging may have application in the early diagnosis of the LV involvements in ARVD.[12,13] Ultrafast computed tomography (UFCT) and magnetic resonance imaging (MRI) have recently come to be accepted as useful noninvasive methods for detection of the myocardial involvements in ARVD.[16–19] There is no report, however, regarding a comparative study of ^{123}I-MIBG imaging with other noninvasive imaging methods in patients with ARVD.

The purpose of this study was to test the feasibility of myocardial ^{123}I-MIBG, ^{201}TlCl, MRI and UFCT for the early detection of LV involvements in ARVD.

MATERIALS AND METHODS

Subjects

Fifteen patients (10 men and 5 women: mean age, 42 years; range, 18 to 66 years) were included in this study. Twelve patients had experienced syncope, and 2 patients had experienced palpitation. In 7 patients medically refractory VT was terminated by cardioversion. ARVD was diagnosed in the presence of documented sustained or nonsustained VT of left bundle branch block morphology, and evidence of characteristic regional severe RV contraction abnormalities (akinesia or dyskinesia) with or without dilatation demonstrated by right ventriculography and radionuclide ventriculography. All patients underwent coronary angiography and had a normal coronary angiogram. Twelve patients had repolarization abnormalities in the right precordial electrocardiographic leads during sinus rhythm (T-wave inversion with excess in lead V_1). Patients with arterial hypertension, diabetes mellitus, coronary artery disease, dilated or hypertrophic cardiomyopathy, congenital or acquired valvular heart disease, or inflammatory heart disease were excluded on the basis of the clinical, echocardiographic, coronary angiographic and radionuclide ventriculographic findings.

Electrophysiological study

An electrophysiological study (EPS) was performed in patients in the non-sedated state not currently receiving anti-arrhythmic drugs whenever possible, by means of a stepwise protocol of programmed ventricular stimulation including single, double and triple extrastimuli during sinus rhythm and ventricular stimulation at two RV stimulation sites (the apex and outflow). If no sustained VT was inducible, the stimulation was repeated during isoproterenol infusion. Endocardial mapping was performed during sinus rhythm and/or during ventricular ectopic activity. The site of origin of VT was defined as the earliest RV local electrocardiogram (ECG) and an identical paced QRS compared with the QRS during VT as verified by 12-lead ECG.

Myocardial imaging of ^{123}I-MIBG and ^{201}TlCl

Image acquisition: In the assessment of myocardial sympathetic nervous activity, ^{123}I-MIBG was injected intravenously (111 MBq), and data were acquired 15 min (early image) and 4 hours (delayed image) after the injection; the delayed image was adopted to allow for

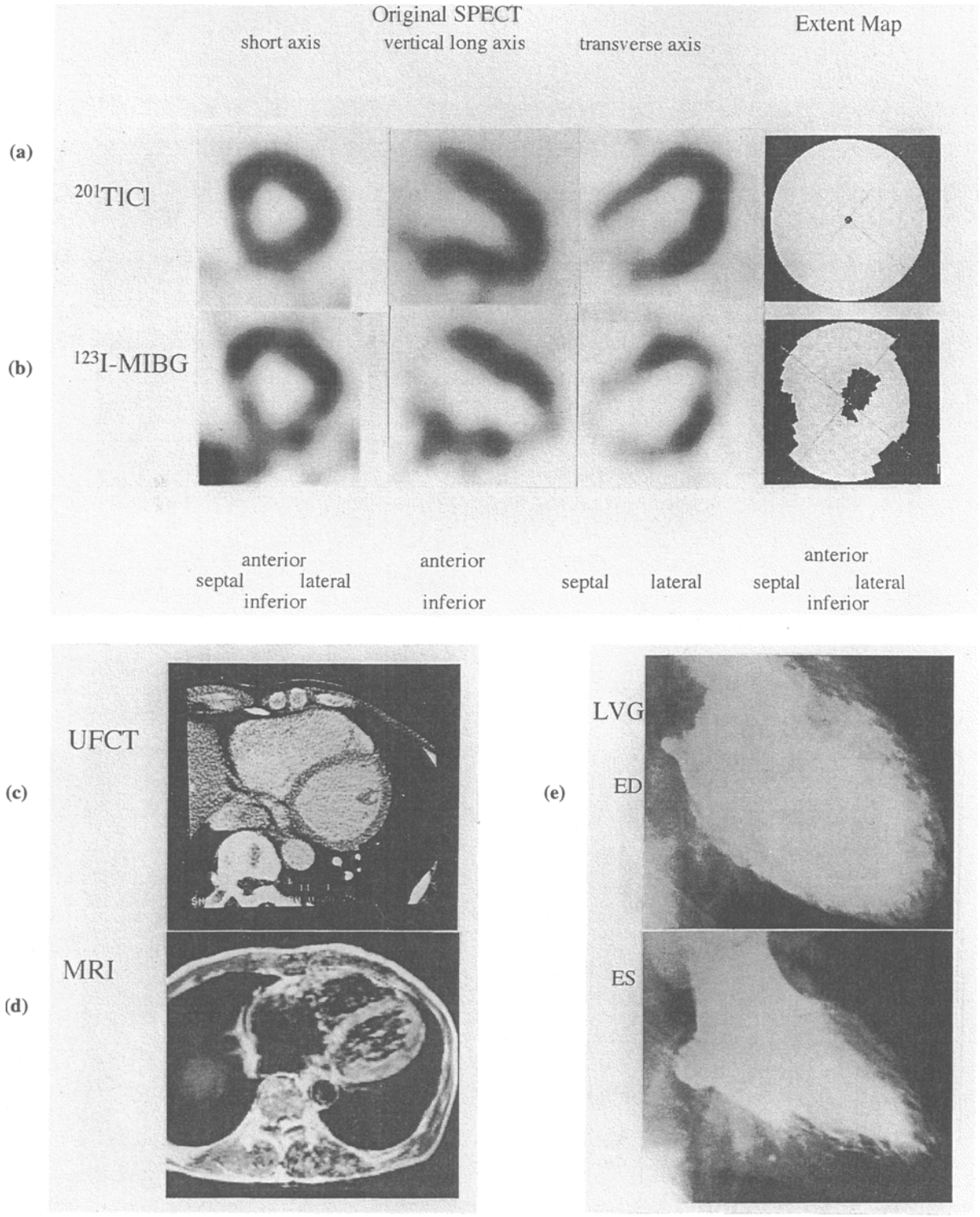

Fig. 1 ^{201}TlCl, ^{123}I-MIBG, UFCT, MRI and left ventriculography in a patient with ARVD (case 2). (a) and (b); There is a normal distribution of ^{201}TlCl, whereas ^{123}I-MIBG images demonstrate reduced tracer uptake in the septal and apical area of LV myocardium. (c) and (d); UFCT and MRI shows normal findings. (e); Left ventriculography shows normal wall motion.

clearance of non-specific tissue uptake. No patient was administered reserpine or tricyclic antidepressants.

^{201}TlCl imaging was performed within 3 days to 3 weeks after the ^{123}I-MIBG study, and only the resting image was obtained. ^{201}TlCl (111 MBq) was intravenously injected, and data were acquired 15 minutes after

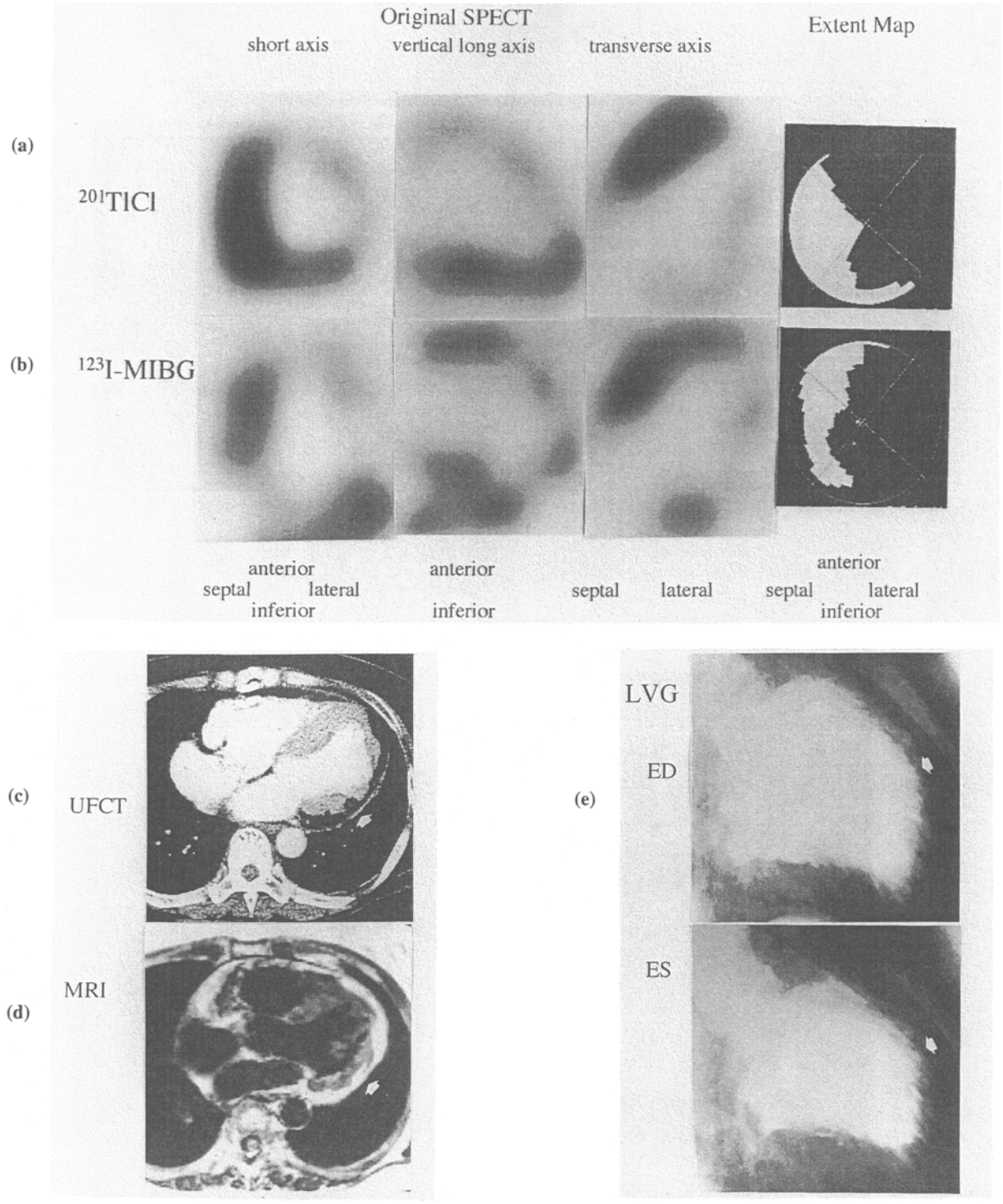

Fig. 2 ^{201}TlCl, ^{123}I-MIBG, UFCT, MRI and left ventriculography in a patient with ARVD (case 13). (a) and (b); There is reduced ^{201}TlCl and ^{123}I-MIBG tracer uptake in the anterior, lateral, and apical areas of the LV myocardium. (c); UFCT shows low density areas in the anterior and lateral walls of left ventricle (arrows in c). The CT number of these areas were –30 Hounsfield units, suggesting fatty tissue. (d); MRI image shows high signal intensity suggesting fatty infiltration in the same areas (arrow in d). (e); Severe hypokinesia is demonstrated in the anterior wall.

the injection. Simultaneous administration and dual-energy acquisition were avoided because of the complexity of the crosstalk fraction between ^{123}I-MIBG and ^{201}TlCl. ^{123}I-MIBG and ^{201}TlCl imagings were performed with a single gamma camera equipped with a low energy general purpose collimator that was interfaced to a minicomputer

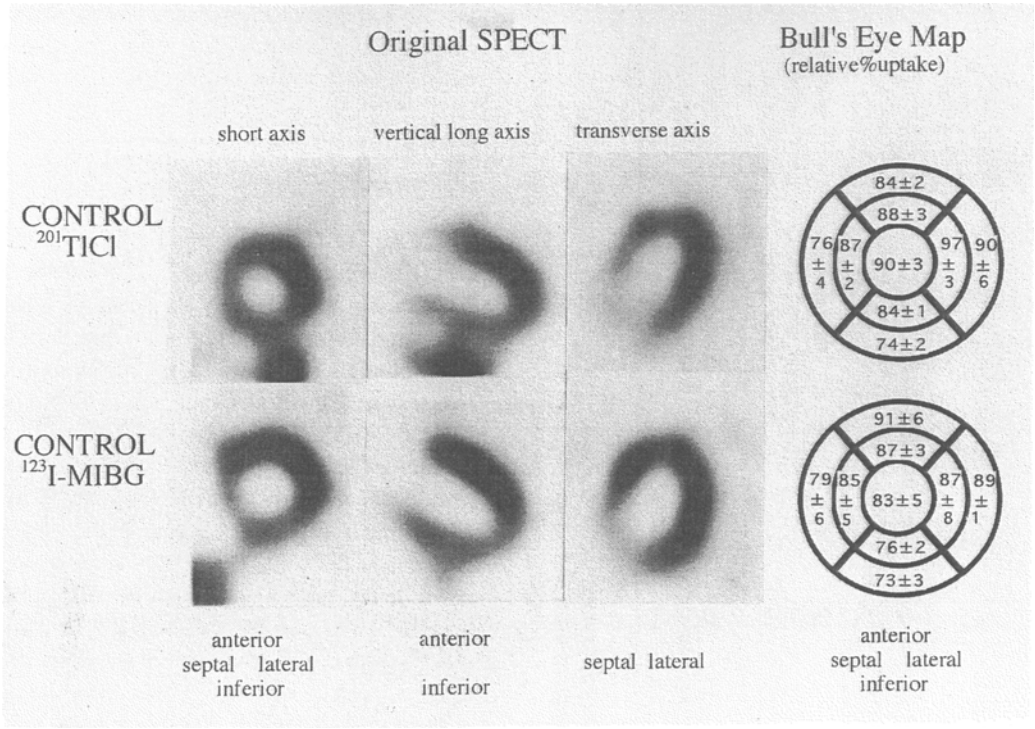

Fig. 3 ^{201}TlCl and ^{123}I-MIBG images of a representative case, and bull's eye map of the relative ^{123}I-MIBG uptake in the control group. There is a homogeneous distribution of ^{201}TlCl and ^{123}I-MIBG. Values are given as mean ± SD.

system (Model GCA901A/HG digital gamma camera and GMS-550U system, Toshiba, Tokyo, Japan). A total of 60 projection images were obtained over 180 degrees in 3-degree increments, at 30 seconds per view in ^{201}TlCl and 45 seconds per view in ^{123}I-MIBG imaging. The data were recorded in 64 × 64 matrices. After preprocessing of the projection images with a Butterworth filter, reconstructed processing was performed by using a Ramp filtered back-projection algorithm. Energy discrimination was centered at 71 KeV with a 20% window for ^{201}TlCl imaging, and at 160 KeV with a 24% window for ^{123}I-MIBG imaging.

Data analysis: The ^{123}I-MIBG uptake of the LV was estimated semiquantitatively with the bull's-eye view setting. Control data were acquired in 10 patients (7 men and 3 women; age range, 23 to 44 years; mean age, 36 years) who were without any evidence of heart disease possibly affecting the sympathetic nervous activity as evaluated by physiological examination, ECG and echocardiography. All of the 10 control patients showed homogeneous distribution of ^{201}TlCl and ^{123}I-MIBG uptake (Fig. 3).[20] The LV was divided into 5 segments, apical, anterior, septal, inferior and lateral. The patients' scans of each segment were visually interpreted by two nuclear medicine physicians taking into consideration the extent score (ES) and severity score (SS) calculated by the following methods.[21]

Extent Score (ES)
= number of abnormal points/total points.
Severity Score (SS)
= Σ (normal count − abnormal count)
in each abnormal point/total points.

Maximum-count circumferential profile analysis is performed every 10 degrees in each of 20 short axis slices. 720 points were equally divided into anterior, septal, inferior and lateral segments. Points having a relative uptake of less than two standard deviations below the mean value for the control group were considered to be abnormal.

Radionuclide ventriculography

We performed radionuclide ventriculography (RNV) in all of the 15 patients to assess RV and LV function. Technetium-99m diethylenetriaminepentaacetic acid human serum albumin (^{99m}Tc-DTPA-HSA, 740 MBq) was injected as an intravenous bolus, and first-pass measurements to calculate the RV ejection fraction (RVEF) were performed in the supine position with the collimator aligned in a 15° to 30° right anterior oblique position. The scan image was acquired with a gamma camera equipped with an all-purpose parallel-hole collimator. Radionuclide counts were collected with a matrix size of 64 × 64 pixels. After an average cycle length was established, gated imaging acquisition was started to calculate the LV ejection fraction (LVEF); every incoming beat was

Table 2 Results of ^{123}I-MIBG and ^{201}TlCl imaging, UFCT, MRI and radionuclide ventriculography

Pt. No.	^{123}I-MIBG imaging						^{201}TlCl imaging						RNV		UFCT		MRI	
	Apic	Ant	Sept	Inf	Lat	ES	SS	Apic	Ant	Sept	Inf	Lat	ES	SS	RVEF	LVEF	RV	LV	RV	LV
1	−	−	−	−	−	6	0	−	−	−	−	−	0	0	42	59	−	−	−	−
2	+	−	+	−	−	20	13	−	−	−	−	−	0	0	37	66	−	−	−	−
3	−	−	+	−	−	14	14	−	−	−	−	−	3	1	41	58	−	−	−	−
4	−	−	−	+	−	21	12	−	−	−	+	−	17	4	19	61	−	−	−	−
5	−	+	−	+	−	10	2	−	+	−	−	−	7	2	23	58	+	−	+	−
6	−	−	+	+	+	23	9	−	−	−	−	+	8	1	56	59	+	−	+	−
7	+	−	−	+	+	22	9	+	−	−	+	+	9	3	45	61	−	−	−	−
8	+	+	+	−	+	35	20	−	+	+	−	−	27	8	44	53	−	−	−	−
9	+	+	+	+	−	55	77	−	−	+	+	−	8	1	22	apic, sept	−	apic, sept	+	apic, sept
10	+	+	+	−	+	26	26	−	−	+	−	−	5	1	33	apic, sept, ant, lat	+	sept, lat	+	sept, lat
11	+	+	+	−	+	29	18	+	+	+	−	+	23	15	18	53	+	apic, sept	+	apic, sept
12	−	−	+	+	+	38	39	−	−	−	+	+	22	4	36	49	+	apic, lat	+	lat
13	+	+	+	+	+	68	153	+	+	+	+	+	65	139	39	41	+	apic, lat	+	apic, lat
14	+	−	+	+	+	59	94	+	−	+	+	+	47	65	30	36	+	apic, sept, inf	+	apic, sept
15	+	+	+	+	+	47	36	+	+	−	+	+	21	10	44	44	−	apic, sept, lat	+	sept, lat

Apic = apical; Ant = anterior; Sept = septal; Inf = inferior; Lat = lateral
SS = severity score calculated from circumferential profile analysis; ES = extent score calculated from circumferential profile analysis;
RNV = radionuclide ventriculography; RVEF = right ventricular ejection fraction (%); LVEF = left ventricular ejection fraction (%)
UFCT = ultrafast computed tomography; MRI = magnetic resonance imaging

sampled, and the cardiac cycle was gated into 20 frames/cycle with a nuclear medicine computer with the patient in the supine position and the collimator aligned in a 30° to 50° left anterior oblique position (the best septal image). The acquisition was stopped when 2,000 counts/frame had been accumulated.

UFCT and MRI imagings

UFCT was performed with a C-100 scanner (Imatron, San Francisco, California). Volume-mode scanning (scanning time, 100 ms for 512 matrix images) was performed in all patients before and after administration of a nonionic contrast medium (Iopamidol 370; Nippon Schering, Osaka, Japan). We first performed serial volume-mode scanning (20 contiguous sections, 6 mm section thickness, 6 mm intervals) at end-systole (40% of RR interval at electrocardiograms) because it was easier to evaluate the ventricular wall. These transverse scans covered the entire heart, with a table incrementation of 6 mm. The scanner table can be inclined 25° in each horizontal direction, and oblique views of the heart on the short or long axis can be obtained, but because the table mobility is limited, neither the short- nor long-axis orientation could be used in this study. The UFCT features were characteristic and consisted of total or partial enlargement of the right ventricle, thinning of the RV or LV walls, evident RV trabeculae, and a marked and localized increase in subepicardial fat demonstrated by means of densitometric analysis.[16]

All MRI studies were performed with a 1.5-T superconducting magnet (Magnetom, Siemens). The imaging sequence used was an ECG-gated spin-echo sequence with a flip angle of 90° and an echo time of 34 ms. With this machine, the minimal time delay is 40 ms for the 90° pulse of selective excitation after the triggering of the R wave on the ECG. The images were acquired in the transverse plane at a slice thickness of 8 mm, and the reconstruction matrix was 256 × 256. The MRI features were characteristic of total or partial enlargement of the right ventricle, thinning of the RV or LV walls, and a marked and localized increase in subepicardial fat, which generates the brightest signal with the spin-echo technique.[18,19,22,23] The UFCT and MRI image findings for each of the 5 segments corresponding to those in ^{123}I-MIBG imaging were assessed separately.

Statistics

Results are shown as the mean ± standard deviation. The Fisher exact test was used to compare categorical variables, and unpaired t-test was used to compare continuous data for the two groups. A p value < 0.05 was considered significant.

RESULTS

Electrophysiological study results

VT originated in the RV outflow tracts in 9 patients, and in the RV inflow tracts in 2 patients (Table 1). Clinical VT was sustained in 11 patients, and nonsustained VT occurred in 4 patients.

Case presentations

Case 1

The myocardial ^{123}I-MIBG, ^{201}TlCl, UFCT and MRI images in Patient 2, with ARVD, are shown in Figure 1. ^{123}I-MIBG defects were demonstrated in the septal and apical areas of the LV myocardium, whereas ^{201}TlCl, UFCT and MRI showed normal findings.

Case 2

The myocardial ^{123}I-MIBG, ^{201}TlCl, UFCT and MRI images in Patient 13, also with ARVD, are shown in Figure 2. Both ^{123}I-MIBG and ^{201}TlCl defects were demonstrated in the anterior, lateral and apical areas of the LV myocardium. UFCT showed low density, the CT number (–30 Hounsfield units) suggesting fatty tissue in the anterior and lateral walls of the LV myocardium. MRI showed high signal intensity in the same areas of the LV myocardium. Severe hypokinesia in the anterior wall was demonstrated by left ventriculography.

Scintigraphic results

In ^{201}TlCl and ^{123}I-MIBG imaging, the right ventricle was not visible in any patient. There was no RV or LV focus of enhanced ^{123}I-MIBG activity ('hot spot') in any patient.

In the early ^{123}I-MIBG imaging, only 4 (27%) of the 15 ARVD patients showed homogeneous tracer uptake, with the remaining 11 patients (73%) showing reduced ^{123}I-MIBG uptake. In the delayed ^{123}I-MIBG imaging, 14 patients (93%) showed regional reduced ^{123}I-MIBG uptake. In 11 patients (73%) with an abnormal ^{123}I-MIBG scan, reduced tracer uptake located in the septal region of the left ventricle was seen. In the resting ^{201}TlCl imaging, 12 patients (80%) showed regional perfusion defects, and all of them showed ^{123}I-MIBG defects. The ES and SS were higher in ^{123}I-MIBG than in ^{201}TlCl imaging (ES: 31.5 ± 18.5 vs. 17.5 ± 18.2, $p < 0.01$, SS: 34.8 ± 42.2 vs. 16.9 ± 37.5, $p < 0.01$). The ^{123}I-MIBG defects were larger and more severe than the ^{201}TlCl defects. Forty-five (60%) of 75 segments showed ^{123}I-MIBG defects, of which 14 (31%) were discordant defects and 31 (69%) were concordant defects (Table 2).

UFCT and MRI findings

Eight patients demonstrated abnormal findings suggesting fatty involvement of the RV myocardium on UFCT or MRI, in 7 of whom such findings were seen on both UFCT and MRI, but none of the 15 patients showed ^{123}I-MIBG uptake in the RV myocardium and abnormalities in the RV myocardium could not be assessed by ^{123}I-MIBG imaging. On both UFCT and MRI, 7 patients (46%) demonstrated abnormal findings suggesting fatty involvement of the LV myocardium, and 14 patients (93%) showed ^{123}I-MIBG defects in the LV myocardium. ^{123}I-MIBG imaging was significantly more sensitive than UFCT and MRI ($p < 0.05$). One patient, an exceptin, had abnormal UFCT findings in the apex of the LV myocardium without abnormal ^{123}I-MIBG and MRI findings (Fig. 4).

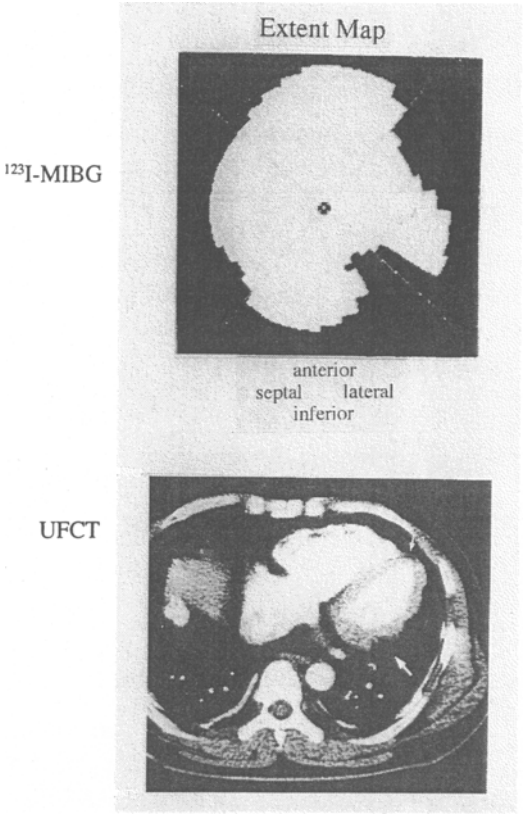

Fig. 4 ^{123}I-MIBG extent map and UFCT images in a patient with ARVD (case 12). UFCT shows low density areas in the apical and lateral wall of LV myocardium (arrows). In ^{123}I-MIBG image, abnormal uptake were demonstrated only in the lateral wall.

Table 3 Comparison of scintigraphic and cardiac systolic functional reults between Group A and Group B

	Group A	Group B	p value
n	7	7	ns
I-123 MIBG			
ES	20.7 ± 7.9	46.0 ± 15.7	$p < 0.01$
SS	11.3 ± 5.5	63.3 ± 48.2	$p < 0.05$
RVEF (%)	37.8 ± 12.9	31.7 ± 9.2	ns
LVEF (%)	59.3 ± 3.6	45.8 ± 5.8	$p < 0.01$

ES = extent score; SS = severity score; RVEF = right ventricular ejection fraction; LVEF = left ventricular ejection fraction

Right and left ventricular Function

All 15 patients underwent radionuclide ventriculography. Fourteen patients had abnormal RVEF (mean RVEF, 35.3%). All 15 patients had localized akinesia, or dyskinesia, and 3 patients had RV dilatation.

Eight patients had abnormal LVEF (mean LVEF, 53.1%), and 3 patients had LV dilatation. Fourteen patients with ^{123}I-MIBG defects were divided into 2 groups of 7 patients each, without abnormal UFCT and MRI findings, suggesting fatty involvement of the LV myocardium (Group A), and 7 with abnormal UFCT and MRI findings (Group B). The ES and SS of ^{123}I-MIBG were larger in Group B than Group A ($p < 0.01$ and $p < 0.05$ irrespectively), and the systolic function as reflected by LVEF was better preserved in Group A ($p<0.01$) (Table 3).

Correlational analysis of results

The analysis of the relation of ^{123}I-MIBG scintigraphic findings to the site of origin of the VT demonstrated reduced septal uptake in 5 (56%) of 9 patients with RV outflow tract origin of the VT, and in both patients with RV inflow tract origins. Both of the latter patients had reduced LVEF, and both had LV involvements demonstrated by UFCT, with large and severe ^{123}I-MIBG defects. In contrast, only 2 (22%) of the 9 patients in the former group had reduced LVEF.

There was no correlation between the results of ^{123}I-MIBG scintigraphy and any of age, history of syncope or cardiac arrest, duration (sustained or nonsustained), RVEF, or biopsy results.

DISCUSSION

In this study, ARVD was diagnosed by observation of sustained or nonsustained VT of left bundle branch block morphology and evidence of characteristic regional RV contraction abnormalities. Abnormal fibrolipomatous infiltration of the RV myocardium was detected by endomyocardial biopsy in 10 patients, and 2 of the other patients showed LV involvements in which the CT number was equal to that of fat as measured by UFCT. It is difficult to distinguish ARVD from RV dilated cardiomyopathy, although regional RV contraction abnormalities and histological characteristics are not suggestive of RV dilated cardiomyopathy.[1,24]

UFCT and MRI have recently come to be used for detection of the myocardial involvements in ARVD,[16–19] and the spatial resolution attained with UFCT or MRI is superior to that of ^{123}I-MIBG imaging. Only 47% of the patients in our study, however, showed abnormal UFCT and MRI findings for the LV myocardium. ^{123}I-MIBG imaging was significantly more sensitive than UFCT and MRI. All patients with abnormal UFCT and MRI findings had abnormal LVEF, and 3 had marked LV dilatation. Functional abnormalities of the LV indicating LV involvement have been observed in the more advanced stage of the disease.[1,25] We speculate that in ARVD the progression of pathophysiological stages in the LV myocardium initially results in ^{123}I-MIBG defects which suggest sympathetic denervation, followed by ^{201}TlCl defects and concordant defects which may suggest transmural fatty infiltration or myocardial fibrosis with associated LV dysfunction, and associated LV dilatation. Lerch and Wichter reported that ^{123}I-MIBG imaging allowed detection of LV adrenergic dysinnervation in ARVD, and, as we found, that ^{123}I-MIBG defects were most frequently detected in the septum and adjacent regions.[12,13] This region is anatomically located adjacent to the right ventricle and closely connected with it via the sympathetic nerve supply. Sympathetic nerve fibers extend through the subepicardial layers, and a dysplastic process might involve the subepicardial layers of the LV in ARVD[1,2]; we speculate that subepicardial dysplastic change may alter or modify autonomic function. ^{123}I-MIBG imaging may therefore be more sensitive in identifying the early stage of LV involvement in ARVD than any other noninvasive imaging method. With this method, we also noted that in one patient, the apical region, in which there were abnormal UFCT findings, could not be detected. Quantitative analysis with the bull's eye map results in under-estimation in the apical region.

Fourteen of our patients had ^{123}I-MIBG defects in the LV myocardium, but none of them had clinical VT of LV origin. In regard to the occurrence of subepicardial dysplastic change in the early stage which might alter the subepicardial sympathetic fibers and may modify autonomic function, there may occur subepicardial sympathetic dysfunction resembling the "denervation supersensitivity" in phenol application, a milieu conducive to the development of VT.[26–28] But because of the degenerative character and massive involvement of fatty infiltration, denervation supersensitivity rather than the effect on a sympathetic imbalance between the normal and hypoinnervated myocardium may contribute to VT.[14] We previously reported that mismatch regions of ^{123}I-MIBG defects with normal ^{201}TlCl uptake were closely connected with the VT origin in dilated cardiomyopathy.[29] In ARVD, we could not obtain direct evidence of any similar relation, because ^{123}I-MIBG could not be detected in the RV. Further examination is needed.

^{123}I-MIBG imaging may be a reliable noninvasive method of detection early in the course of ARVD. UFCT and MRI may be useful in the detection of abnormal findings in patients who show LV dysfunction with advanced fatty infiltration and fibrosis.

REFERENCES

1. Marcus FI, Fontaine GH, Guiraudon G, Frank R, Laurenceau JL, Malergue C, et al. Right ventricular dysplasia. A report of 24 adult cases. *Circulation* 65: 384–398, 1982.
2. Fontaine G, Fontaliran F, Linares-cruz E, Chomette G,

Grosgogeat Y. *Cardiac Arrhythmias; Recent Progress in Investigation and Management.* Elsevier Science Publishers, pp. 189–202, 1988.
3. Furlanello F, Bettini R, Bertoldi A, Vergara G, Visona L, Durante GB, et al. Arrhythmia patterns in athletes with arrhythmogenic right ventricular dysplasia. *Eur Heart J* 10 (suppl D): 16–19, 1989.
4. Wichter T, Borggrefe M, Haverkamp W, Chen X, Breithardt G. Efficacy of antiarrhythmic drugs in patients with arrhythmogenic right ventricular disease: results in patients with inducible and noninducible ventricular tachycardia. *Circulation* 86: 29–37, 1992.
5. Glowniak JV, Turner FE, Gray LL, Palac RT, Lagunas-Solar MC, Woodward WR. Iodine-123 metaiodobenzylguanidine imaging of the heart in idiopathic congestive cardiomyopathy and cardiac transplants. *J Nucl Med* 30: 1182–1191, 1989.
6. Gohl K, Feistel H, Weikl A, Bachmann K, Wolf F. Congenital myocardial sympathetic dysinnervation (CMSD)—a structural defect of idiopathic long QT syndrome. *Pace* 14: 1544–1553, 1991.
7. Kline RC, Swanson DP, Wieland DM. Myocardial imaging in man with I-123-metaiodobenzylguanidine. *J Nucl Med* 22: 129–132, 1981.
8. Merlet P, Valette H, Dubois-Rande J-L, Moyse D, Duboc D, Dove P, et al. Prognostic value of cardiac metaiodobenzylguanidine imaging in patients with heart failure. *J Nucl Med* 33: 471, 1992.
9. Stanton MS, Touli MM, Radtke NL. Regional sympathetic denervation after myocardial infarction in humans detected noninvasively using I-123 metaiodobenzylguanidine. *J Am Coll Cardiol* 14: 1519–1526, 1989.
10. Stark RP, McGinn AL, Wilson RF. Chest pain in cardiac-transplant recipients. *N Engl J Med* 324: 1791–1794, 1991.
11. Wellman HN, Zipes DP. Cardiac sympathetic imaging with radioiodinated metaiodobenzylguanidine (MIBG). *Prog cardiol* 3: 161–174, 1989.
12. Lerch H, Bartenstein P, Wichter T, Hindricks M, Borggrefe G, Breithardt G, et al. Sympathetic innervation of the left ventricle is impaired in arrhythmogenic right ventricular disease. *Eur J Nucl Med* 20: 207–212, 1993.
13. Wichter T, Hindricks G, Lerch H, Bartenstein P, Borggrefe M, Schober O, et al. Regional myocardial sympathetic dysinnervation in arrhythmogenic right ventricular cardiomyopathy: an analysis using ^{123}I-meta-iodobenzylguanidine scintigraphy. *Circulation* 89: 667–683, 1994.
14. Wichter T, Borggrefe M, Breithardt G. Die arrhythmogene rechtsventrikulare Erkrankung. *Z Kardiol* 80: 107–125, 1991.
15. Pinamonti B, Salvi A, Silvestri F, Sinagra G, Camerini F. Left ventricular involvement in right ventricular cardiomyopathy. *Eur Heart J* 10 (suppl D): 20–21, 1989.
16. Hamada H, Takamiya M, Ohe T, Ueda H. Arrhythmogenic right ventricular dysplasia: evaluation with electron-beam CT. *Radiology* 187: 723–727, 1993.
17. Sotozono K, Imahara S, Masuda H, Akashi K, Kamegai M, Miyake F, et al. Detection of fatty tissue in the myocardium by using computerized tomography in a patient with arrhythmogenic right ventricular dysplasia. *Heart Vessels Suppl* 5: 59–61, 1990.
18. Klersy C, Raisaro A, Salerno JA, Montemartini C, Campani R. Arrhythmogenic right and left ventricular disease: evaluation by computed tomography and nuclear magnetic resonance imaging. *Eur Heart J* 10 (suppl D): 33–36, 1989.
19. Casolo GC, Poggesi L, Boddi M, Fazi A, Bartolozzi C, Lizzadro G, et al. ECG-gated magnetic resonance imaging in right ventricular dysplasia. *Am Heart J* 113: 1245–1248, 1987.
20. Stirner H, Buell U, Kleinhans E. Three-dimensional ROI-based quantification of stress/rest ^{201}Tl myocardial SPET: presentation of method. *J Nucl Med* 25: 128–133, 1986.
21. Kubota M. Quantitative assessment of infarct size with the unfolded map method of ^{201}Tl myocardial SPECT in patients with acute myocardial infarction. *KAKU IGAKU (Jpn J Nucl Med)* 29: 333–346, 1992.
22. Suzuki J, Sakamoto T, Takenaka K, Kawakubo K, Amano K, Takahashi H, et al. Assessment of the thickness of the right ventricular free wall by magnetic resonance imaging in patients with hypertrophic cardiomyopathy. *Br Heart J* 60: 440–445, 1988.
23. Suzuki J, Sakamoto T, Takenaka K, Amano K, Amano W, Igarashi T, et al. New subtype of apical hypertrophic cardiomyopathy identified with nuclear magnetic resonance imaging as an underlying cause of markedly inverted T waves. *J Am Coll Cardiol* 22: 1175–1181, 1993.
24. Fichett DH, Sugrue DD, Macarthur CG, Oakley CM. Right ventricular dilated cardiomyopathy. *Br Heart J* 51: 25–29, 1984.
25. Manyari DE, Klein GJ, Gulamhusein S, Boughner D, Guiraudon GM, Wyse G, et al. Arrhythmogenic right ventricular dysplasia: a generalised cardiomyopathy? *Circulation* 68: 251–257, 1983.
26. Zipes DP. Ischemic modulation of myocardial innervation. *G Ita Cardiol* 22: 615–621, 1992.
27. Mitrani DR, Klein LS, Miles WM, Burt RW, Wellman HN, Zipes DP. Regional cardiac sympathetic denervation in patients with ventricular tachycardia in the absence of coronary artery disease. *J Am Coll Cardiol* 22: 1344–1353, 1993.
28. Inoue H, Zipes DP. Results of sympathetic denervation in the canine heart: supersensitivity that may be arrhythmogenic. *Circulation* 75: 877–887, 1987.
29. Maeno M, Ishida Y, Shimonagata T, Hayashida K, Toyama T, Hirose Y, et al. The significance of ^{201}Tl/^{123}I-MIBG (metaiodobenzylguanidine) mismatched myocardial regions for predicting ventricular tachycardia in patients with idiopathic dilated cardiomyopathy. *KAKU IGAKU (Jpn J Nucl Med)* 30: 1221–1229, 1993.